IEEE Access
Multidisciplinary | Rapid Review | Open Access Journal

Received September 22, 2018, accepted October 14, 2018, date of publication October 25, 2018,
date of current version November 30, 2018.

Digital Object Identifier 10.1109/ACCESS.2018.2877799

Investigation of Impact Loads Caused by Ultrasonic Cavitation Bubbles in Small Gaps

FUSHI BAI[1], KAI-ALEXANDER SAALBACH[1], LIANG WANG[1,2], AND JENS TWIEFEL[1]

[1]Institute of Dynamics and Vibration Research, Leibniz Universität Hannover, 30167 Hannover, Germany
[2]State Key Laboratory of Mechanics and Control of Mechanical Structures, Nanjing University of Aeronautics and Astronautics, Nanjing 210016, China

Corresponding author: Fushi Bai (baifushi@hotmail.com)

This work was supported by the Open Access Fund of the Leibniz Universität Hannover.

ABSTRACT Ultrasonic cavitation shows a great potential in various industrial applications such as sonochemistry, food processing, ultrasonic cleaning, and surface treatments. These applications have the advantages of high temperatures or high pressure due to the collapse of cavitation bubbles. In surface treatments, the collapse of bubbles occurs near workpiece surfaces and creates micro-jets which lead to high impact forces. As one of these surface treatment processes, ultrasonic cavitation peening requires a small gap between the vibration source and the treated surface to obtain the maximum impact force. Due to these small gaps, the growth and collapse of cavitation bubbles are affected, which result in the changes of impact forces. Therefore, the investigation of the impact loads caused by ultrasonic cavitation bubbles in small gaps is the focus of this contribution. A theoretical model taking into consideration bubble interactions is utilized to estimate the optimal standoff distance at which the largest impact forces occur. Then, experimental investigations are carried out. A piezoelectric sensor with a titanium alloy cover is used to record the number of impacts and their amplitudes. The recorded signals are then processed in time and frequency domains. The experimental results show that large impact loads are generated when the gap width is in the range of 0.5–0.8 mm. It is also found that the maximum working efficiency occurs in this range.

INDEX TERMS Cavitation bubbles, impact loads, small standoff distance, working efficiency.

I. INTRODUCTION

Ultrasonic cavitation is widely used in industrial applications such as sonochemistry, food processing, ultrasonic cleaning, surface treatments and so on [1], since the cavitation bubbles can generate high temperatures and high-pressures after collapsing [2]. In most applications, the growth and collapse of cavitation bubbles are not limited or only limited by a rigid wall. However, in some surface treatment applications, especially for ultrasonic cavitation peening, the cavitation bubbles are limited in small gaps to achieve high impact loads on the workpiece surface and ensure less energy loss in the bubbly liquid [3]. During ultrasonic cavitation peening, the sonotrode is generally partly immersed in liquid and cavitation bubbles are generated in the small gap between the tip end and the surface of workpiece. The gap width is defined as the standoff distance [4] and is usually less than 1 mm [5]. After the cavitation bubble collapse, high impact forces (loads) on the workpiece surface are generated due to the micro-jets [6]. As a result, plastic deformation is generated, which is beneficial for enhancing the surface hardness, improving the compressive residual stress of the metal surface and extending the life of high loading parts [7]. Furthermore, ultrasonic cavitation peening has many advantages: its compact structure, it is easy to control and produces less pollution [8]. Therefore, ultrasonic cavitation peening is considered as a potential surface enhancement technology. Apart from the applications of ultrasonic cavitation peening, ultrasonic cleaning also uses a small standoff distance of around 1 mm to remove the contaminants [12].

During ultrasonic cavitation peening, the impact load caused by the bubble collapse plays an important role in the improvement of the treatment surface. Through the measurement of the total surface deformation, the effects of the impact during ultrasonic cavitation peening were evaluated [9]. However, it is difficult to obtain the impact number and impact loads. The surface deformation also caused the change in the distribution of cavitation bubbles. Cavitation pitting is another way to evaluate the cavitation impact loads. Due to the hydrodynamic impact loads caused by cavitation bubble collapses, some pits are generated on the treated

surface. These cavitation pits can be utilized as the signals of the impact loads and controlled by the material's constitutive behavior [10]. By analyzing the numbers of pits per unit surface region, the cavitation intensity or aggressiveness are determined. In the pit measurement, it is proposed that the single pit is generated by one impact load. For the pit measurement, aluminum alloy, duplex stainless steel, and Nickel-Aluminum Bronze can be used as the target material to predict the impact loads [11]. This method is limited by the material characteristics and cannot precisely evaluate the cavitation intensity due to the overlap of the impact loads in the same area.

In order to record the impact signals on the treated surface, piezoelectric effects can be utilized [12], as piezoelectric sensor can provide more information about impact loads, including the amplitude of impact loads and the number of the impact loads. During measurement, the impact signals are converted directly into the electric signals due to the piezoelectric effects. Thus, by analyzing the electric output the impacts caused by bubble collapses can be shown clearly. Franc *et al.* [21] used a commercial piezoelectric pressure sensor to measure the impact loads in a cavitation flow. The measurement results revealed a simple exponential law that depends on a reference peak and a reference load. Although the pressure sensors are easy to operate and have high measurement accuracy, the sensor surfaces undergo severe erosion especially during high power cavitation. A PVDF (Polyvinylidene Fluoride) sensor was also developed to evaluate the cavitation impact energy. In this kind transducer, two layers of tape were attached to the front side and an acrylic resin, the acoustic impedance of which was almost equal to PVDF, was glued on the back side [13]. However, this transducer has a large attenuation of the measured signals and the tape is easily destroyed if the cavitation intensity is strong enough.

Although the impact loads caused by cavitation bubbles near a rigid wall were widely investigated, a study of the number and the amplitude of the impact loads caused by ultrasonic cavitation bubbles in a small gap is has not yet been conducted. Taking the bubble interactions into account, a model on the prediction of the largest impact on treatment surface under different process parameters can be calculated. To validate the simulation results, a piezoelectric sensor is used to capture the impact signals. A titanium alloy cover of the sensor is used to prevent extensive erosion. Then, the effects of different standoff distances and driving currents on the impact loads are analyzed and discussed in both time domain and frequency domain. The treatment efficiency under different operation parameters is finally discussed in detail.

II. SIMULATION OF THE OPTIMAL STANDOFF DISTANCE

The aim of this section is to provide a theoretical analysis in order to obtain the largest impact load at different standoff distances and vibration amplitudes. Due to the effects of bubbles and bubble interactions, the properties of sound propagation are changed, which can be calculated firstly. Then the sound pressure in small gaps is obtained. At last the maximum bubble size which generates the largest impact load is simulated. Based on the classical model provided by Van Wijngaarden [16], the complex wavenumber k_m in bubbly liquid can be calculated by Equation (1):

$$k_m^2 = \frac{\omega^2}{c^2} + 4\pi\omega^2 \int_0^\infty \frac{af(a)}{\omega_0^2 - \omega^2 + 2ib\omega} da \tag{1}$$

In this equation, ω is the frequency of the wave and c is the sound speed in the pure liquid. a is a bubble radius. The equilibrium radius is calculated by a Gaussian distribution $f(a)$. ω_0 and b are the resonance frequency of bubbles and the damping factor, respectively.

Fuster *et al.* [15] used the potential I_0 from surrounding bubbles to modify the classic model in order to consider the interactions of bubbles. Then, the modified complex wavenumber k_m is obtained as in the method described by Jamshidi *et al.* [14]. Using the modified complex wavenumber, the sound pressure distribution in a small gap is modeled as follows.

In the model of the sound field in a small gap, the tip end of the sonotrode is considered a flat disk and vibrates harmonically, generating a sound beam as a sound source. Then, the beam travels though the bubbly liquid and is reflected by the treated surface. The reflected wave goes back to the tip end of the sonotrode and is reflected again and again until the wave totally dissipates in the bubbly liquid. The sound source is subdivided into many point sources and constrains the radiation into the half-space with the entire acoustic energy. Therefore, the sound pressure at any point M in the bubbly liquid can be calculated by Equation (2) [17]. The point source is considered as the infinitesimal area dS'. The distance from point M to the source is $\mathbf{r}'_\mathbf{M}$ while to the center of the flat disc is $\mathbf{r}_\mathbf{M}$.

$$p(\mathbf{r}_\mathbf{M}) = \frac{i\omega\rho}{2\pi} u_0 \iint_{S'} \frac{e^{i(k|\mathbf{r}'_\mathbf{M} - \mathbf{r}_\mathbf{M}|)}}{|\mathbf{r}'_\mathbf{M} - \mathbf{r}_\mathbf{M}|} dS' \tag{2}$$

where u_0 is the peak amplitude of the transducer velocity, p is the pressure at point M.

The bubbly liquid is considered a liquid with a homogeneous distribution of cavitation bubbles due to the small standoff distance while the workpiece surface is considered a rigid wall which is infinite and directly converts the wave propagation direction. The sound field calculated from Equation (2) is overlaid with the reflection sound filed. The sound pressure is overlapped again and again until the sound pressure tends to zero. Therefore, the acoustic field with the consideration of bubble interactions is simulated. All the values of the physical parameters used in the model are shown in Table 1 [19].

In the previous studies, the relationship between sound pressure and bubble size was determined [18] and it was concluded that the largest impact occurs when the standoff distance equals the diameter of the maximum bubble size [5].

TABLE 1. Values of the physical parameters used in the model.

Physical parameters	Unit	Values
Density	ρ (kg/m^3)	998.21
Surface tension coefficient	σ (N/m)	0.07236
coefficient of viscosity	μ (Pa/s)	0.001
Static pressure	P_0 (Pa)	1.013×10^5
Vapor pressure	P_{ge} (Pa)	2.34×10^3
polytropic exponent	K	1
Sound speed of the host liquid	c (m/s)	1500
Ratio of specific heats	γ	1.4
Gas thermal diffusivity	D (m^2/s)	2.4×10^{-4}

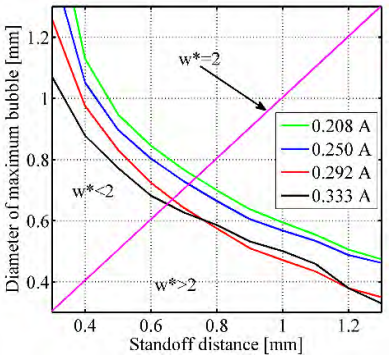

FIGURE 1. Bubble size at different standoff distances and driving currents.

Thus, the distribution of bubble size on the treated surface at different standoff distances and driving currents can be obtained by combining the results of [5] and [18]. Here w^* is defined as the ratio of the standoff distance L to the corresponding diameter of the maximum bubble R_m. In the case of $w^* = 2$, the largest impact is generated when the cavitation bubble collapses. Since the largest cavitation bubble causes the largest impact on the treated surface, the strongest sound pressure is used in the following calculations.

From Fig. 1, it can be seen that there is a line intersecting the four curves. The intersection points represent the case of $w^* = 2$. The area above the line denotes the case of $w^* < 2$. In this area, the cavitation bubbles are not spherical due to the limitation of the small gap, which leads to the decrease of the impact load on the treated surface. The area below the line represents the case of $w^* > 2$. In this area, the cavitation bubbles that came into contact with the treated surface are spherical and their diameters are less than the gap width. As a result, the impact loads on the treated surface decreases as well. Therefore, the standoff distances at which the largest impact occurs are 0.75 mm, 0.73 mm, 0.68 mm and 0.67 mm, corresponding to the driving currents of 0.208 A, 0.250 A, 0,292 A and 0.333 A, respectively. The vibration amplitude

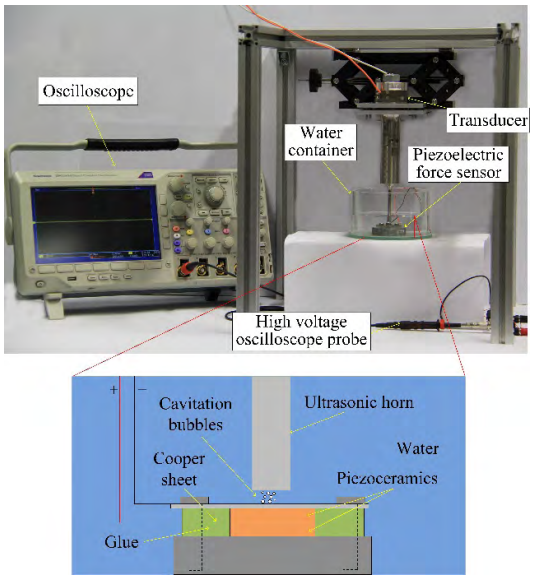

FIGURE 2. Experimental setup for detecting impact utilizing piezoelectric sensor.

at the end surface of the sonotrode is linearly proportional to the driving current with a ratio of 120 μm/A [9].

In conclusion, due to the limitations of rigid walls and the attenuation, there is a bubble with a diameter equal to the standoff distance in certain sound pressures. It is deduced that a fixed vibration amplitude corresponds to an optimal standoff distance. With the increase in the vibration amplitude, the sound pressure near the treated surface decreases correspondingly due to the high attenuation. The bubble size will decrease as well, which leads to the decrease in the optimal standoff distance.

III. EXPERIMENTS

The experimental setup for impact detection and the piezoelectric sensor are illustrated in Fig. 2. The transducer is a classical sandwich transducer driven by a digital phase and amplitude control unit at its longitudinal eigenmode [9]. The resonance frequency is about 23 kHz. The sonotrode with the tip diameter of 5 mm is made of titanium alloy. During measurements, the resonance frequency and the driving current of the transducer were recorded by an oscilloscope (Tektronix DPO3014). A piezoelectric sensor was adhered to the bottom of a water container. The piezoelectric sensor consists of a titanium alloy surface cover, two piezoelectric disks and an aluminum alloy bottom. The diameter and the thickness of the piezoelectric disk were 12 mm and 2 mm. The thickness of the surface cover is 0.5 mm. There is a copper sheet between the two piezoelectric ceramics as the positive electrode. Waterproof glue was used to keep water out of the piezoelectric disks. The signals from the sensor were converted first by a high voltage oscilloscope probe (100x attenuation Testec TT-HV) and then recorded by the oscilloscope. The sampling frequency is 500 kHz. The signals were recorded at a sampling rate of 10 M/s with a duration of 20 s. Since the resistance of the probe is as high

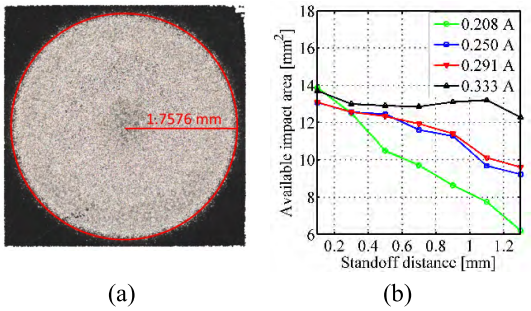

FIGURE 3. (a) The radius of the cavitation erosion area and (b) the available impact area at different driving currents and standoff distances.

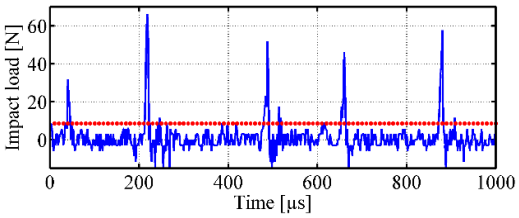

FIGURE 4. Peak amplitudes and peak width on the processed signal.

as 100 MΩ, the impedances of other parts in the electric circuit can be ignored. In the measurements, the standoff distance changed from 0.1 mm to 1.3 mm with an interval of 0.1 mm. The experiments were carried out at the driving current of 0.208 A, 0.25 A, 0.292 A and 0.333 A, respectively.

The piezoelectric sensor was calibrated using a steel ball impact method [20]. During the calibration, a steel ball was hung by a string, which can be considered as a simple pendulum. The piezoelectric sensor was erected and hit by the steel ball. A high speed camera was used to record the movement of the ball while an oscilloscope was utilized to record the output signals. It is assumed that the lost kinetic energy of the ball after the collision is totally converted into the electric energy. The relationship between the output voltage of the piezoelectric sensor V_B and the impact force F_B can be described as:

$$V_B = 0.694 F_B \frac{V}{N} \tag{3}$$

where, V and N are the units of voltage and force, respectively.

In order to evaluate the available impact area on the treatment surface, aluminum alloy specimens with polished surfaces were treated by ultrasonic cavitation at different driving currents and standoff distances. The erosion area on the treated surface can reflect the available impact area, as shown in Fig. 3 (a). Fig. 3 (b) shows the available impact area at different treatment conditions.

IV. RESULTS AND DISCUSSION

With the impact caused by the bubble collapse, the electric signals generated by the piezoelectric sensor are recorded. Fig. 4 shows a part of the impact load signals which are converted by the electric signals using Equation (3).

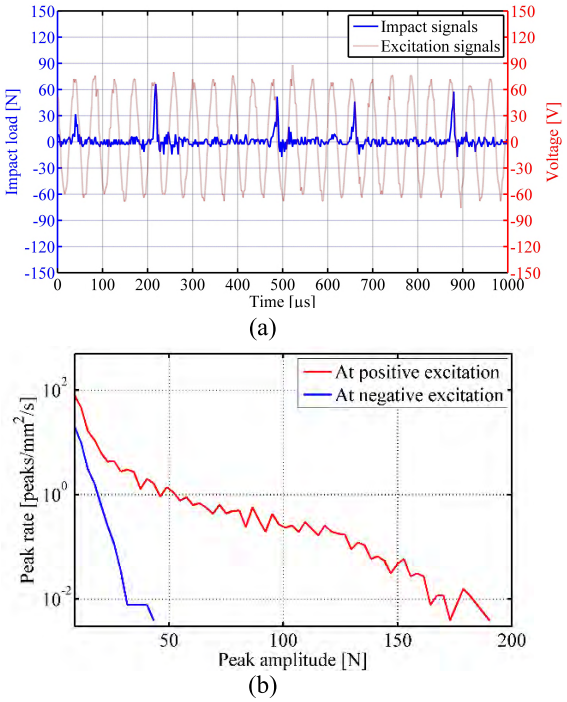

FIGURE 5. (a) Example of the impact signals and the excitation signals; (b) The peak rate corresponding to the positive peaks and negative peaks of the excitation signals.

The Aluminum foil is used to detect the minimum threshold of the impact loads, since an impact load below this value which just damages the Aluminum foil is not expected to cause any damage to other metal materials. The value of the threshold is 8.6 N and shown as the red dashed line, which is much larger than the background noise (maximum value: 0.0058 N). Additionally, ΔT is defined as the peak width. In the following time domain analysis, only the peaks whose amplitudes exceed 8.6 N are considered.

The growth and collapse of cavitation bubbles follow the variations of the sound pressure in a liquid. The positive pressure in the liquid corresponds to the positive excitation signals of the transducer. Thus, the variations of bubbles change periodically with the vibration of sonotrode. Fig. 5 (a) partly shows both the excitation signals and the impact loads simultaneously in the case of the driving current of 0.333 A and the standoff distance of 0.7 mm. It can be seen that that the larger impact peaks mainly occur at the positive excitation signals but are not generated in every excitation period. The positive and negative excitation mean the positive and negative driving voltages, respectively. The reason for this is that the larger impact loads may be caused by the bubble clusters which are not generated every period. Fig. 5 (b) shows that peaks at the maximum positive pressure are more numerous and larger than that at the maximum negative pressure, which means that the larger impacts on the treatment surface are mainly generated in the period of positive excitation.

A. ANALYSIS IN TIME DOMAIN

Due to the piezoelectric effect, the higher impact load peaks are caused by more violent bubble collapses. In Fig. 6 the

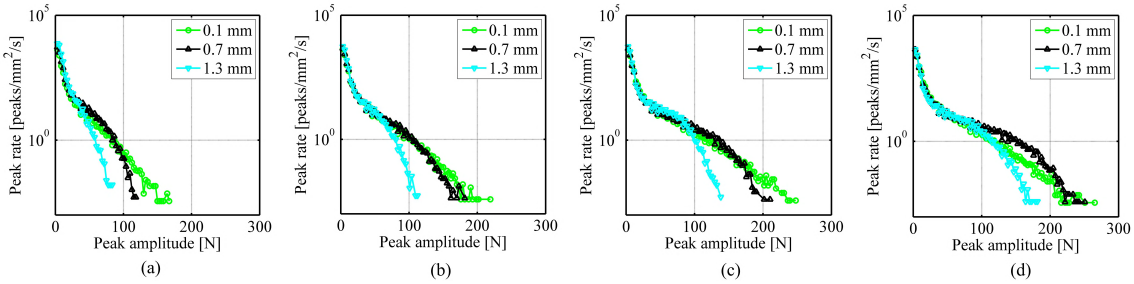

FIGURE 6. Frequency distribution of load peak at the driving currents of (a) 0.208 A, (b) 0.250 A, (c) 0.291 A and (d) 0.333 A.

distributions of peak rates are processed at different driving currents (0.208 A, 0.250 A, 0.292 A and 0.333 A) and standoff distances (0.1 mm, 0.7 mm, 1.3 mm). The higher impact loads occur at the higher driving currents, since higher driving currents results in an increase in sound energy on the sensor surface. In particular, the number of cavitation bubbles generated on the sensor surface at higher driving currents is more than that at smaller driving currents, which means that the impact loads increase due to more overlapping impulses and more cavitation clusters. The peak rate and peak amplitude change greatly with the variations of the standoff distance. As show in Fig. 6, at the same driving current, the impact loads increase and then decrease with increasing standoff distance. This is because the highest impact load occurs in the case of around $w^* = 2$. With smaller standoff distances, the growth and collapses of cavitation bubbles are limited while with larger standoff distances, the bubbles near the sensor surface become smaller due to attenuation of sound propagation. These figures also show that the amplitude of most peaks does not exceed 50 N. When the amplitude of the impact loads is larger than 50 N, the frequency of the higher impact loads is higher at the higher driving current. This phenomenon additionally shows that higher driving currents introduce more cavitation clusters.

The peak width is another factor key to evaluating the impact loads caused by cavitation bubbles, as longer peak durations cause more impact energy on the sensor surface. As shown in Fig. 7, the peak rate decreases with the increase in the peak width. The change tendency almost keeps similar with increasing the peak width even though the driving current and the standoff distance change. Therefore, the peak width has less influence on the impact loads than on the treatment surfaces.

The impacts at different conditions can be illustrated by the peak amplitude, peak width and peak number. The results can be fitted by a line function, as this is an easy way to reflect the relationship between the peak amplitude, peak width and peak number. Through the fitted line, the concentrated area of the peaks can be determined. The larger value of the slope of the fitted line means that the peak amplitudes are higher at the same peak width compared to the smaller value of the slope. In Fig. 8 (a), an example of the fitted line at the driving current of 0.208 A and at the standoff distance of 0.1 mm is shown. Thus, the greater the value of the slope,

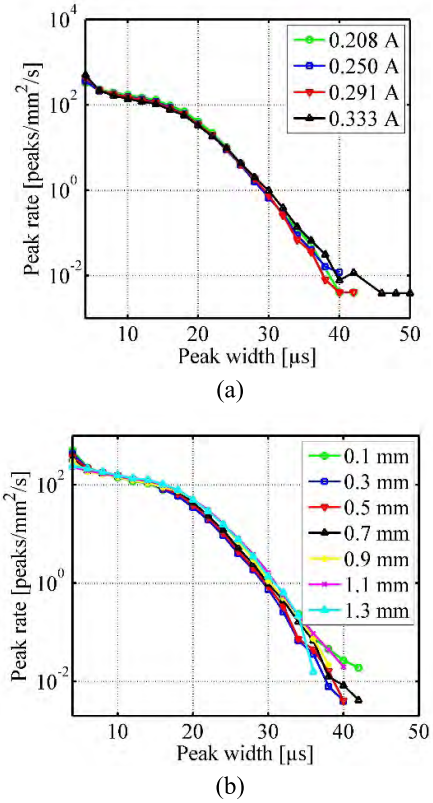

FIGURE 7. Peak rate versus peak width at different driving currents and standoff distances.

the higher impact on the treated surface. It can be seen that with the increase in the driving current, the impact loads on the surface increase. At the same driving current, when the standoff distance increases the impact on the treated surface increases and then decreases. The optimal standoff distance occurs at the range of 0.6 mm and 0.9 mm.

Since the impact loads caused by the collapse of cavitation bubbles show the periodicity characteristics, in the following section the impact signals can be processed in frequency domain, whereby new characteristics are found.

B. ANALYSIS IN FREQUENCY DOMAIN

The cavitation bubbles grow and collapse periodically when the sonotrode is driven at the resonance frequency of about 23 kHz. To identify the underlying characteristics of the impact loads, the signals captured from the piezoelectric

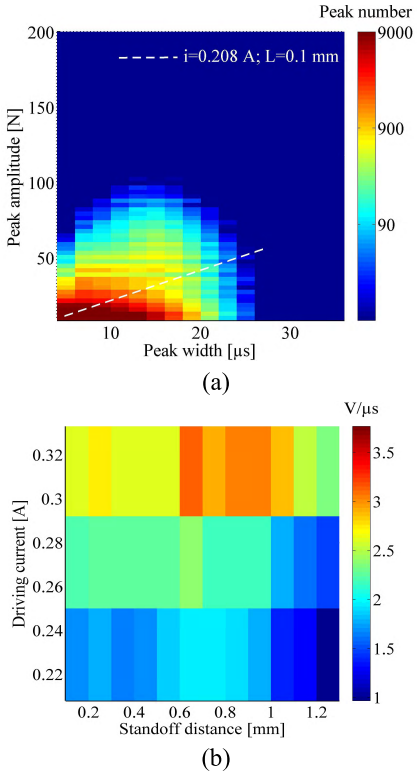

FIGURE 8. (a) An example of the fitted line and (b) the slopes of the fitted lines at different driving currents and standoff distances.

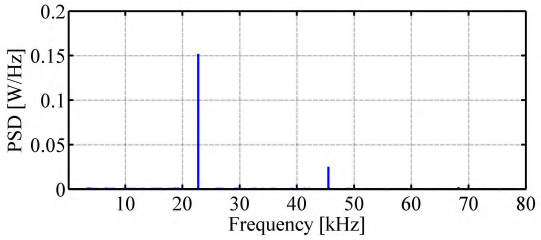

FIGURE 9. Power spectrum density at the standoff distance of 1. mm and at the driving current of 0.333 A.

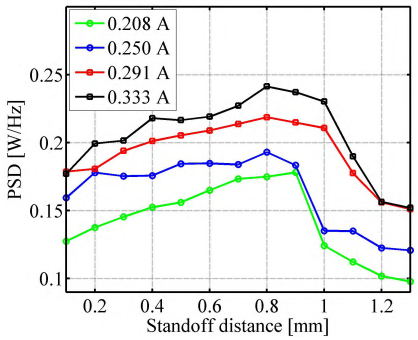

FIGURE 10. The amplitude of the power spectrum density at the resonance frequency of 23 kHz.

sensor are analyzed by the power spectrum density (PSD). In the PSD analysis, the bandwidth of the power is from 0 to 10^5 Hz. The frequency resolution is 0.02 Hz. For qualitative analysis, it is usually assumed that the resistance R_e is 1 Ω to get the normalized power value. Then, the de-normalized power value can be obtained by substituting in the actual power value. The signal sequences are computed utilizing the Matlab implementation of the Welch method which is a commonly used estimation method for correcting the power spectral density with 50% overlap. A flattop window function of 2.5 s size is used to compensate for the spectral energy leaks. Since the resistance of the high voltage probe in the circuit is 100 MΩ, the recorded signals can be considered as the power signals generated directly from the sensor. The original unit of the PSD is V^2/Hz. Due to the normalized effect, the unit can transform V^2/Hz into $V^2/\Omega/Hz\,(W/Hz)$. An example at the standoff distance of 1.3 mm and at the driving current of 0.333 A is shown in Fig. 9. It can be seen that the largest peak is located at about 23 kHz, which causes the main effects on the sensor surface. The peaks at around 46 kHz and 69 kHz are caused by the effects of the sound irradiation from the second collapses of the cavitation bubbles. Because the greatest effect is caused at the frequency of about 23 kHz, in the analysis of the frequency domain only the PSD at this frequency is taken into account.

Fig. 10 shows the amplitude of the power spectrum density at about 23 kHz with the variations of the driving current and the standoff distance. Similar to the tendency shown in Fig. 8 (b), the amplitude value of PSD increases with the increase in the driving current while the amplitude value increases first and then decreases with the increase in the standoff distance. The difference is the range of the optimal standoff distance between 0.8 mm and 0.9 mm, because the results only show the main power at the resonance frequency. Nevertheless, the analysis in frequency domain is easily to conduct.

C. EFFICIENCY ANALYSIS

Since the impact loads at other frequencies in frequency domain also influence the treatment surface, the total received power of the piezoelectric sensor needs to be analyzed. The total received power is the sum of the power at each frequency. The power at a given frequency can be obtained from PSD. For the purpose of industrial application, the efficiency is an essential factor to be investigated. The ratio of the total received power to the input electric power of transducer is defined as the efficiency. Fig. 11 (a) shows the input power which is applied on the working transducer in different conditions. The high driving current causes higher input power while the standoff distance has less influence on the input power. Fig. 11 (b) shows the efficiencies at different driving currents and different standoff distances. It can be seen that at low driving currents the efficiency is higher than that at higher driving currents, because the attenuation is less at small driving current due to low vapor volume fraction in the liquid. In the case of $w^* = 2$, the highest efficiency occurs.

From the analysis of the impact in the time and frequency domains, the optimal standoff distance is obtained when the ultrasonic cavitation occurs at small standoff distances. The efficiency is also investigated in different standoff distances and driving currents. These investigations can be used

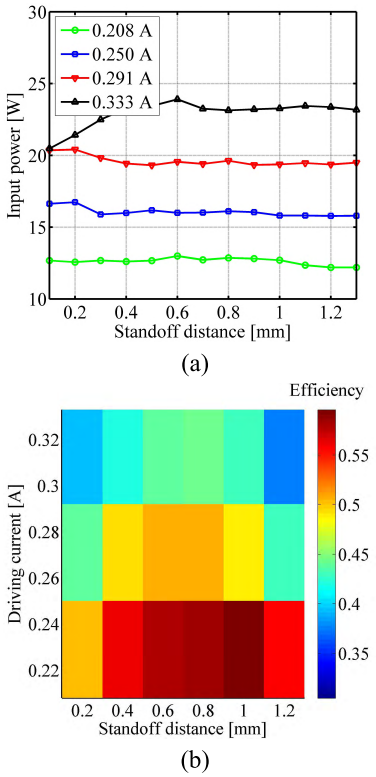

FIGURE 11. (a) Input power of the transducer at different driving currents and standoff distance; (b) Efficiency at different driving currents and standoff distances.

as a guideline for the ultrasonic cavitation process during which the high impact loads are required.

V. CONCLUSION

In this work, the number and amplitude of the impact loads, as well as the process efficiency, are investigated at different driving currents and distances. The optimal standoff distance is studied both theoretically and experimentally. The simulation results show that the greatest impact on the sensor surface occurs in the range of 0.67 mm and 0.75 mm under the investigation conditions. Through the experimental investigation, it is found that higher driving currents cause higher impact loads while the largest impact loads occur approximately at the optimal standoff distance. Due to the higher attenuation caused by higher driving currents, the efficiency at higher driving currents is lower than that at lower driving currents. These studies provide theoretical and experimental evidence for the ultrasonic cavitation process during which high impact loads are required.

REFERENCES

[1] G. Harvey, A. Gachagan, and T. Mutasa, "Review of high-power ultrasound-industrial applications and measurement methods," *IEEE Trans. Ultrason., Ferroelectr., Freq. Control*, vol. 61, no. 3, pp. 481–495, Mar. 2014.
[2] V. N. Khmelev, S. N. Tsyganok, Y. M. Kuzovnikov, V. A. Shakura, M. V. Khmelev, and S. S. Zorin, "Study of ultrasonic cavitation action on the process of part cleaning from burrs," in *Proc. 17th Int. Conf. Young Specialists Micro/Nanotechnol. Electron Devices (EDM)*, Erlagol, Russia, 2016, pp. 275–279.
[3] Y. Gao, B. Wu, Y. Liu, Y. Zhou, N. Shen, and H. Ding, "Ultrasonic cavitation peening of stainless steel and nickel alloy," *J. Manuf. Sci. Eng.*, vol. 136, no. 1, pp. 014502-1–014502-5, Feb. 2014.
[4] F. Bai, K.-A. Saalbach, J. Twiefel, and J. Wallaschek, "Effect of different standoff distance and driving current on transducer during ultrasonic cavitation peening," *Sens. Actuators A, Phys.*, vol. 261, pp. 274–279, Jul. 2017.
[5] F. Bai, K.-A. Saalbach, Y. Long, J. Twiefel, and J. Wallaschek, "Capability evaluation of ultrasonic cavitation peening at different standoff distances," *Ultrasonics*, vol. 84, no. 1, pp. 38–44, Mar. 2018.
[6] A. Shima, K. Takayama, Y. Tomita, and N. Miura, "An experimental study on effects of a solid wall on the motion of bubbles and shock waves in bubble collapse," *Acta Acustica United Acustica*, vol. 48, no. 5, pp. 293–301, Aug. 1981.
[7] M. R. Sriraman and R. Vasudevan, "Influence of ultrasonic cavitation on surface residual stresses in AISI 304 stainless steel," *J. Mater. Sci.*, vol. 33, no. 11, pp. 2899–2904, Jun. 1998.
[8] D. G. Shchukin, E. Skorb, V. Belova, and H. Möhwald, "Ultrasonic cavitation at solid surfaces," *Adv. Mater.*, vol. 23, no. 17, pp. 1922–1934, May 2011.
[9] F. Bai, K.-A. Saalbach, L. Wang, X. Wang, and J. Twiefel, "Impact of time on ultrasonic cavitation peening via detection of surface plastic deformation," *Ultrasonics*, vol. 84, no. 1, pp. 350–355, Mar. 2018.
[10] A. Jayaprakash *et al.*, "Scaling study of cavitation pitting from cavitating jets and ultrasonic horns," *Wear*, vol. 296, nos. 1–2, pp. 619–629, Aug. 2012.
[11] S. C. Roy, J. P. Franc, and M. Fivel, "Cavitation erosion: Using the target material as a pressure sensor," *J. Appl. Phys.*, vol. 118, no. 16, pp. 164905-1–164905-11, Oct. 2015.
[12] B. Verhaagen and D. F. Rivas, "Measuring cavitation and its cleaning effect," *Ultrason. Sonochem.*, vol. 29, pp. 619–628, Mar. 2016.
[13] H. Soyama, Y. Sekine, and K. Saito, "Evaluation of the enhanced cavitation impact energy using a PVDF transducer with an acrylic resin backing," *Measurement*, vol. 44, no. 7, pp. 1279–1283, Aug. 2011.
[14] R. Jamshidi, B. Pohl, U. A. Peuker, and G. Brenner, "Numerical investigation of sonochemical reactors considering the effect of inhomogeneous bubble clouds on ultrasonic wave propagation," *Chem. Eng. J.*, vols. 189–190, no. 3, pp. 364–375, May 2012.
[15] D. Fuster, J. M. Conoir, and T. Colonius, "Effect of direct bubble-bubble interactions on linear-wave propagation in bubbly liquids," *Phys. Rev. E, Stat. Phys. Plasmas Fluids Relat. Interdiscip. Top.*, vol. 90, no. 6, p. 063010, Dec. 2014.
[16] L. Van Wijngaarden, "On the equations of motion for mixtures of liquid and gas bubbles," *J. Fluid Mech.*, vol. 33, no. 3, pp. 465–474, Sep. 1968.
[17] S. W. Dähnke and F. J. Keil, "Modeling of linear pressure fields in sonochemical reactors considering an inhomogeneous density distribution of cavitation bubbles," *Chem. Eng. Sci.*, vol. 54, nos. 13–14, pp. 2865–2872, Jul. 1999.
[18] S. Dähnke and F. J. Keil, "Modeling of three-dimensional linear pressure fields in sonochemical reactors with homogeneous and inhomogeneous density distributions of cavitation bubbles," *Ind. Eng. Chem. Res.*, vol. 37, no. 3, pp. 848–864, Mar. 1998.
[19] H. Lin, B. D. Storey, and A. J. Szeri, "Inertially driven inhomogeneities in violently collapsing bubbles: The validity of the Rayleigh–Plesset equation," *J. Fluid Mech.*, vol. 452, pp. 145–162, Feb. 2002.
[20] Y.-C. Wang and Y.-W. Chen, "Application of piezoelectric PVDF film to the measurement of impulsive forces generated by cavitation bubble collapse near a solid boundary," *Exp. Thermal Fluid Sci.*, vol. 32, no. 2, pp. 403–414, Nov. 2007.
[21] J. P. Franc, M. Riondet, A. Karimi, and G. L. Chahine, "Impact load measurements in an erosive cavitating flow," *J. Fluids Eng.*, vol. 133, no. 12, p. 121301, Dec. 2011.

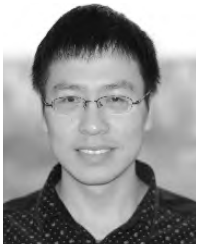

FUSHI BAI received the M.Sc. degree in mechanical engineering from Sichuan University in 2014. He is currently pursuing the Ph.D. degree with the Piezoelectrics and Ultrasonics Workgroup, Institute of Dynamics and Vibration Research, Leibniz University Hannover. He mainly focuses on ultrasonic cavitation and peening process.

KAI-ALEXANDER SAALBACH has been a Research Engineer with the Piezoelectrics and Ultrasonics Workgroup, Institute of Dynamics and Vibration Research, Leibniz University Hannover, since 2011. His primary areas of research are ultrasonic levitation, ultrasonic assisted hybrid casting, and cavitation research.

LIANG WANG received the B.E. degree in detection guidance and control technology and the M.Sc. degree in mechanical engineering from the Nanjing University of Aeronautics and Astronautics, China, in 2012 and 2015, respectively, where he is currently pursuing the Ph.D. degree with the State Key Laboratory of Mechanics and Control of Mechanical Structures. He had an abroad study experience with Leibniz University Hannover (LUH), Germany, from 2013 to 2014. He is a Visiting Ph.D. Candidate with the Institute of Dynamics and Vibration Research, LUH. His research interests include piezoelectric ultrasonic actuators and their applications.

JENS TWIEFEL received the Ph.D. degree from Leibniz Universität Hannover in 2010. He is the Leader of the Piezoelectrics and Ultrasonics Workgroup, Institute of Dynamics and Vibration Research, Leibniz University Hannover.